Genetic Evidence that SOST Inhibits WNT Signaling in the Limb

Nicole M. Collette[1,2], **Damian Genetos**[3], **Deepa Murugesh**[1,2], **Richard M. Harland**[2], and **Gabriela G. Loots**[1,2,*]

[1]Biology and Biotechnology Division, Lawrence Livermore National Laboratory, 7000 East Avenue, L-452, Livermore, CA 94550

[2]Department of Molecular and Cell Biology, Division of Genetics, Genomics, and Development, and Center for Integrative Genomics, University of California, Berkeley, CA 94720-3204, USA

[3]Department of Surgical and Radiological Sciences, School of Veterinary Medicine, University of California, Davis, CA 95616, USA

Abstract

SOST is a negative regulator of bone formation and mutations in human *SOST* are responsible for sclerosteosis. In addition to high bone mass, sclerosteosis patients occasionally display hand defects, suggesting that *SOST* may function embryonically. Here we report that overexpression of *SOST* leads to loss of posterior structures of the zeugopod and autopod by perturbing anterior-posterior and proximal-distal signaling centers in the developing limb. Mutant mice that overexpress *SOST* in combination with *Grem1 and Lrp6* mutations display more severe limb defects than single mutants alone, while *Sost$^{-/-}$* significantly rescues the *Lrp6$^{-/-}$* skeletal phenotype, signifying that *SOST* gain-of-function impairs limb patterning by inhibition of WNT signaling through LRP5/6.

Keywords

WNT signaling; SOST; Sclerostin; Shh; Limb formation

Introduction

Sclerosteosis is an autosomal recessive form of generalized hyperostosis (MIM 239100) due to hyperactive osteoblast activity that results from loss of sclerostin or SOST expression. Targeted deletion of *Sost* in mice causes increased bone formation and bone strength, and administration of anti-sclerostin antibodies increases bone formation and restores bone loss in osteoporotic rats (Li et al., 2008a; Li et al., 2008b). For a minority of sclerosteosis patients, syndactyly of digits (Cremin, 1979) has been described primarily as asymmetric cutaneous syndactyly of the index and middle fingers (digits 2 and 3). Furthermore, some patients have remarkably deformed fingers with hypoplasia and nail dysplasia (symmetric or asymmetric) most commonly associated with the index finger (Cremin, 1979). We have previously reported that elevated levels of human *SOST* in transgenic mice cause a decrease in bone and mineral density in the appendicular and axial skeleton. We also noted that these mice display varying degrees of digit abnormalities ranging from fused and split to missing digits (Loots et al., 2005). While originally *SOST* was thought to primarily function in the adult skeleton as an

*Author for correspondence (loots1@llnl.gov).

osteocyte-secreted factor that negatively regulates bone formation (Balemans et al., 2001; Brunkow et al., 2001; Li et al., 2008a; van Bezooijen et al., 2004) and promotes osteoblast apoptosis (Sutherland et al., 2004), the hand abnormalities described for sclerosteosis patients along with the gain-of-function limb defects suggest that *SOST* may also function embryonically, during limb and hand formation.

Based on sequence similarity, SOST was originally identified as a member of the DAN family of cysteine-rich BMP-antagonists that include DAN, Cerberus, GREM1, DAND5 (CERL2, DANTE, COCO) and its paralog SOSTDC1 (Brunkow et al., 2001; Yanagita, 2005). While BMP2, 4 and 7 are largely dispensable for limb patterning (Bandyopadhyay et al., 2006), exogenous BMPs have been shown to affect the size and shape of long bones, by increasing the recruitment of progenitor mesenchymal stem cells into the chondrogenic lineage (Duprez et al., 1996; Macias et al., 1997). However, both noggin and gremlin, which encode antagonists of BMP signaling, are essential for proper skeletal patterning (Benazet et al., 2009; Brunet et al., 1998; Khokha et al., 2003).

Similarly, WNT signal transduction is essential for limb development (Holmen et al., 2004; Pinson et al., 2000). Several WNTs have been shown to control early events during proximal-distal outgrowth and dorso-ventral limb patterning as well as participate in later events during chondrogenesis, osteogenesis, muscle development, and joint formation. Mutations in human *WNT3* and *WNT7A* result in severe skeletal malformations (Niemann et al., 2004; Woods et al., 2006) and several mouse lines have been described where misregulation of WNT signaling causes limb defects (Galceran et al., 1999; Parr and McMahon, 1995). Like BMP signaling, WNT signaling is also attenuated at the receptor level by two types of regulatory proteins. Secreted frizzled related proteins (SFRP) directly bind to WNT ligands and prevent them from binding to the receptor, while members of the Dickkopf family (DKK) interact with the two WNT co-receptors, low density lipoprotein receptor-related proteins 5 and 6 (LRP5/6) (Niehrs, 2006; Pinzone et al., 2009). The balance between ligands and antagonists modulate the inputs of WNT signaling and subsequently contribute to proper limb outgrowth, patterning and cartilage differentiation.

Examination of SOST and its paralog, SOSTDC1 has revealed that these molecules can behave both as BMP-(Kassai et al., 2005; Laurikkala et al., 2003; Winkler et al., 2003) and WNT-antagonists (Ellies et al., 2006; Itasaki et al., 2003; van Bezooijen et al., 2004; van Bezooijen et al., 2007; Lin et al., 2009), generating some uncertainty about their molecular action, *in vivo*. Our previous work has described a transgenic mouse that overexpressses human *SOST* from a bacterial artificial chromosome, where elevated levels of *SOST* cause osteopenia; we also noted that these mice display limb defects. In the current study we have investigated the role of SOST in limb pattering through genetic and molecular analyses of AER, ZPA and limb-specific markers of BMP and WNT signaling pathways to understand the underlying mechanism of SOST action in the developing limb. In addition to evidence that *SOST* overexpression inhibits WNT/β-catenin signaling *in vivo*, we find that overexpression of *SOST* in $Sost^{tg}$;$Lrp6^{+/-}$ mice modifies the otherwise phenotypically wildtype $Lrp6^{+/-}$ limb to mimic the *Lrp6* knockout limb phenotype, while the removal of *Sost* in $Sost^{-/-}$;$Lrp6^{-/-}$ double knockouts significantly rescues $Lrp6^{-/-}$ skeletal phenotypes, supporting a primary role for SOST in the inhibition of the WNT signaling pathway during the initial stages of limb bud formation, and a critical role for ectodermal derived WNT signaling in the establishment of both the zone of polarizing activity and the apical ectodermal ridge.

Results and Discussion

Characterization of limb defects in Sost gain-of-function embryos

We have previously reported that increased SOST expression in transgenic mice (*Sost^{tg}*) carrying a ~158 kb human BAC (Fig. 1A) led to low bone mass in the appendicular and axial skeleton (Loots et al., 2005). The observed osteopenia was shown to be gene dose-dependent, such that transgenic mice with higher levels of *SOST* exhibited a more dramatic decrease in tibial cancellous bone volume. *Sost^{tg}* transgenics also displayed gene-dose dependent limb abnormalities ranging from missing digits, fused and split digits to loss of posterior bone structures (Loots et al., 2005; Fig. 1B and Sup. Fig. 1B, Fig. 2). In severely affected embryos, the limb bud appeared developmentally delayed and misshapen as early as E9.5, with truncation along the A-P axis, resulting in a cylindrical limb bud with reduced AER on the posterior side (Fig. 1c,d). By E12.5 we observed abnormal chondrocyte condensation of skeletal structures, and the formation of the phalanges was also delayed, with reduced separation or lack of digit formation. By E14.5, in most severely affected embryos the ulna was absent, and digits 2 to 5 often failed to form (Sup. Fig. 1A).

Scoring of 117 neonates [77 *Sost^{tg}* and 40 wildtype; derived from *Sost^{tg}* × *Sost^{tg}* and *Sost^{tg}* × wt matings] revealed that *Sost* gain-of-function most dramatically perturbs the autopod and zeugopod patterning along the A-P axis, where digit 5 (the most posterior autopod skeletal structure) was missing in 87% of *Sost^{tg}* embryos. The ulna was absent from at least one forelimb in 22% of the *Sost^{tg}* embryos, and 11% of *Sost^{tg}* embryos completely lacked all autopod and zeugopod skeletal elements. The humerus and scapula were never affected, even in the most severe cases (Fig. 1B). We also observed a left-right asymmetry, such that the left forelimb and right hindlimb were more severely affected (Sup. Fig. 1B). To correlate the severity of digit abnormality with BAC copy number or zygosity we examined human *SOST* expression in E11.5 limb buds derived from matings of phenotypically normal but hemizygous parents. Following Mendelian ratios, 25% of embryos were genotypically wildtype and 75% were *Sost^{tg}*. On average, one third of *Sost^{tg}* limb buds were affected (resembling the embryo depicted in Fig 1e; top panel) and the rest were phenotypically wildtype (resembling the embryo depicted in Fig 1e; bottom panel). Using quantitative rtPCR we examined human *SOST* expression levels in pooled *Sost^{tg}* embryos, and found 100% of the affected embryos to have ~2× the amount of human *SOST* expression detected in phenotypically normal *Sost^{tg}* embryos, confirming that the severity of limb defects correlates with Mendelian inheritance ratios, BAC zygosity and human *SOST* expression levels (Sup. Fig. 2).

To examine whether human *SOST* was expressed according to the morphological changes in limb patterning, as well as whether it faithfully recapitulated the endogenous mouse *Sost* expression, we used *in situ* hybridization in wildtype or human *SOST* transgenic mice and β-galactosidase activity in mice where murine *Sost* has been replaced by *LacZ*. Supporting the validity of the *LacZ* expression, we found the knock-in expression to recapitulate mouse *Sost* expression monitored by *in situ* hybridization but with better signal to noise ratio (Sup. Fig. 3E, F); therefore we used *LacZ* embryos to monitor mouse *Sost* expression. For both human and mouse *Sost* we observed a dynamic pattern of expression that began during the initial stages of limb bud formation [~27-somite stage], where *Sost* was found to be expressed throughout the dorsal and ventral limb ectoderm (Fig. 1; Fig. 2Q; Sup. Fig. 3). At E10.5 the expression was significantly higher on the ventral side, extended proximally to the trunk, while on the dorsal side it was concentrated more distally, but excluded from the AER (Fig. 1d-f). This pattern continued until E12.5, when expression became distally restricted, though *SOST* expression continued to be excluded from the AER (Fig. 1f). Generally, murine and transgenic human *SOST* expression mirrored each other, with slight qualitative differences (Sup. Fig. 3), while quantitatively (using quantitative rtPCR) we found endogenous mouse *Sost* expression to be 2-fold less than transgenic human *SOST* expression in defective embryos (Sup. Fig. 2).

To ensure the limb defects observed in *Sost^tg* embryos result from high levels of *SOST* in its endogenous expression domain, rather than spatiotemporal misexpression of human *SOST*, we examined *Sost^tg*;*Sost^-/-* embryos. We anticipated that limb defects resulting from an overdose will be fully or partially rescued by the lack of mouse *Sost* in *Sost^-/-* embryos. All *Sost^tg*;*Sost^-/-* embryos examined (N=9) were fully rescued. Among *Sost^tg*; *Sost^+/-* embryos 60% (N=21) were fully normal and 40% (N=14) had mild digit abnormalities (Table S1), suggesting that *Sost^-/-* complements the limb defects caused by *SOST* overexpression in *Sost^tg* transgenic embryos.

Repression of ZPA and AER genes in Sost^tg limb buds

The loss of posterior skeletal elements observed in severely affected *Sost^tg* animals (Fig. 1B) was highly reminiscent of two mutant strains: *Wnt7A* (Parr and McMahon, 1995) and *Shh* (Kraus et al., 2001) where digits 2-5 and the ulna were absent, while other proximal skeletal elements were unaffected. This suggested that elevated levels of SOST interfere either with establishing or maintaining the ZPA function to regulate digit formation and identity through the SHH morphogen (Ahn and Joyner, 2004;Kraus et al., 2001). Similar to *limb buds deficient in Wnt7a*, which is also expressed in the ectoderm, *Shh* expression was dramatically reduced in *Sost^tg* limb buds (Fig. 2A-D). The decrease in *Shh* expression was variable from embryo to embryo, consistent with the range of loss of posterior skeletal elements observed in older animals (9/9 defective and 4/9 phenotypically normal *Sost^tg* embryos showed reduced *Shh* limb expression by *in situ* hybridization). Despite ectodermal restriction of *Sost* expression and absence from the AER (Fig. 2Q; Sup. Fig. 3), AER gene expression was also affected in *Sost^tg* and *Sost^-/-* embryos. Both *Fgf4* (Fig. 2E-H) and *Fgf8* (Fig. 2I-L) were down regulated in *Sost^tg* (11/11 defective and 7/13 normal *Sost^tg* embryos showed reduced *Fgf4* limb expression by *in situ*; 12/12 defective and 9/18 normal *Sost^tg* embryos showed reduced *Fgf8* limb expression by *in situ*). In particular, both *Fgf*-4 and -8 expression domains were narrower along the dorsoventral axis in *Sost^tg* limb buds (Fig 2F′,J′; red arrow) and wider in *Sost^-/-* limb buds (Fig 2G′, K′; green arrow), suggesting that Sost contributes to the establishment of the AER domain. While *in situ* hybridization revealed a dorso-ventral expansion of the *Fgf8* domain in *Sost^-/-* embryos (Fig. 2K′), quantitative measurements (by quantitative rtPCR) showed *Fgf8* mRNA to be also reduced in embryos lacking *Sost* (Fig. 2L), possibly due to loss of *Fgf8* expression in the anterior AER (Fig 2K; black arrows). Despite the observed dorso-ventral expansion, we attributed the decrease in *Fgf8* expression in *Sost^-/-* embryos to the weaker expression per cell and a more restricted anterior-posterior expression domain.

Although loss of *Shh* has been reported to result in decreased *Grem1* expression levels (Litingtung et al., 2002) at E10.5 (Fig. 2P), we found no quantitative change in *Grem1* expression in *Sost^tg* embryos. However, the *Grem1* expression domain expanded posteriorly into the region that lacks *Shh* positive cells (Fig 2N, N′; red arrow), consistent with the observation that *Shh* descendants lack the ability to express *Grem1* (Scherz et al., 2004) (Fig. 2M-O). We also observed a strong shift in *Grem1* expression domain on the ventral side (the dorsal side was unaffected) where *Sost* expression is the highest (Fig. 2Q), where in both *Sost^tg* (Fig 2N′) and *Sost^-/-* (Fig. 2O′) embryos *Grem1* expression was excluded from the anterior region.

Genetic evidence of SOST as a WNT inhibitor

SOST was initially characterized as a BMP- antagonist, and more recently as a WNT antagonist. To determine if SOST favors the inhibition of BMP, WNT, or both of these pathways, in the limb, we examined genetic interactions between *Sost* gain- and loss-of-function alleles and *Grem1*, *Lrp5* or *Lrp6* knockout alleles. The protein products of these genes are well-established components of the canonical BMP- and WNT-signaling pathways,

respectively, and these mutants show limb defects of a similar nature to those observed in the *Sost* gain-of-function transgenic mice.

We reasoned that if secretion of SOST and GREM1 proteins primarily inhibit BMP signaling in the adjacent AER through epithelial-mesenchymal interactions (Michos et al., 2004; Panman et al., 2006), they may have redundant functions during limb patterning, such that elevated levels of *SOST* would potentially rescue the *Grem1*^{-/-} phenotype. Our rationale was based on the observation that both Noggin and Gremlin are BMP antagonists expressed in the limb bud which have the ability to interchangeably rescue gene expression changes in the limb bud of *ld* mutant mice (Khokha et al., 2003; Zuniga et al., 1999), yet their physiological roles in the limb bud are different, and their null phenotypes are distinctive (Brunet et al., 1998; Khokha et al., 2003; Zuniga et al., 1999). Alternatively, if *SOST* inhibits the canonical WNT-pathway through one or both of the LRP-receptors, elevated levels of *SOST* would modify the *Lrp5* and *Lrp6* limb knockout phenotypes. We found that elevated *SOST* expression fails to rescue but rather exacerbates the *Grem1*^{-/-} phenotype where 40% of *Sost*[tg];*Grem1*^{-/-} embryos (4 of 10) lack most autopod structures, and the zeugopod consists of a truncated bone fused to a dramatically shortened humerus (Fig. 3D; Table 1), indicating that *Sost* and *Grem1* are not acting in the same molecular pathway.

In contrast, we found that SOST shows strong interactions with the WNT pathway, consistent with SOST acting as a WNT inhibitor *via* its interactions with the WNT co-receptors LRP5 and LRP6 (Ellies et al., 2006; Itasaki et al., 2003; Li et al., 2005). Reduction of LRP function results in limb defects (Holmen et al., 2004) such that 35% of *Lrp5*^{+/-};*Lrp6*^{+/-} and 72% of *Lrp5*^{-/-};*Lrp6*^{+/-} are affected, where the severity follows the left to right and anterior-posterior axis, highly similar to *Sost*[tg] phenotype (Fig. 1B, Fig. 3, and Table 1). Consistent with the idea that LRP6 is the more important receptor in the embryo, *Lrp6*^{-/-} mutants display strong effects in the limb, while *Lrp5*^{-/-} limbs develop normally. We found that *Sost*[tg];*Lrp6*^{+/-} mice have enhanced limb abnormalities closely resembling those of *Lrp6*^{-/-} limbs, relative to either *Lrp6* heterozygotes, which look phenotypically normal, or *Sost*[tg] strain, suggesting that SOST inhibits LRP5/6 receptors (Fig. 3F). 20% of *Sost*[tg];*Lrp6*^{+/-} embryos also displayed spina bifida and tail truncation phenotypes similar to *Lrp6*^{-/-} homozygotes (Table 1; data not shown) suggesting that SOST also inhibits WNT signaling in the nervous system, consistent with *Sost* expression pattern (Fig. 1C, D, E). In addition we, observed a mild enhancement of the *Sost*[tg] phenotype when LRP5 was reduced in *Sost*[tg]; *Lrp5*^{-/-} embryos (Table 1) as further evidence that SOST interacts with both LRP5 and LRP6 co-receptors during limb development.

We also reasoned that elimination of the putative WNT antagonist SOST would elevate WNT signaling and rescue the limb phenotypes of *Lrp5/6* mutants. *Lrp6*^{-/-} forelimbs have a dramatically shortened zeugopod with one bone and two digits (Fig. 3E) while the hindlimbs lack the autopod and fibula, and show fused hip bones (Fig. 3J). We found *Sost*^{-/-};*Lrp6*^{-/-} mice to have significantly rescued skeletons, where the forelimbs lack only digit 5 (Fig. 3H, compare to 3E). A more dramatic rescue was observed in the hindlimbs, where the absence of SOST resulted in hindlimbs that lack only 1-2 digits (Fig. 3K), in contrast to the complete lack of autopods in *Lrp6*^{-/-} mice. Though reduced in size, the fibula was also restored in these animals, and the ilium bones were fully separated. *Lrp6*^{-/-} mice also have small heads, small eyes (microophthalmia), cleft upper and lower lips, lack tails, and display different degrees of spina bifida (Pinson et al., 2000). The removal of SOST in *Sost*^{-/-};*Lrp6*^{-/-} mice ameliorated some of these defects (Sup. Fig. 4), but the most dramatic rescue was evident in the appendicular skeleton, where SOST rescued the hand and feet defects (Fig.3H,K); this evidence demonstrates that SOST genetically interacts with the WNT signaling pathway during limb and skeletal development. Mechanistically, the loss of SOST, which normally interferes with WNT signaling, releases inhibition on other LRP receptors (possibly LRP5), allowing them to compensate for and partially rescue the complete loss of LRP6 receptor. In contrast, removing

SOST in *Sost^-/-*;*Grem1^-/-* double knockouts did not rescue *Grem1^-/-* autopod defects (data not shown).

Disruption of ectodermal and mesnchymal WNT signaling in the Sost^tg limb bud

To determine whether both *Sost^tg* and *Lrp6^-/-* limb defects may be mediated by the same direct or indirect molecular perturbations, we compared transcript levels in E10.5 forelimb buds of several key regulators thought to be involved in our model of WNT antagonism. We found levels of *Shh* and its target gene *dHand* to be ~20% and ~50% of normal expression in both *Sost^tg* and *Lrp6^-/-* limb buds (Fig. 4A,B). To determine whether both *Sost^tg* and *Lrp6^-/-* defective limbs both have reduced WNT signaling activity, we used quantitative rtPCR to examine expression of Axin2, a direct target of Wnt/β-catenin signaling (Jho et al., 2002). *Axin2* transcript levels were significantly decreased in in *Sost^tg* and *Lrp6^-/-* mutant limb buds (Fig. 4C), adding to the evidence that SOST inhibits the canonical WNT-pathway in the limb.

Furthermore, we quantified transcript levels of 168 genes related to WNT and BMP function using quantitative rtPCR arrays (Sup. Table 2). Nine genes were down-regulated ≥1.5 fold in *Sost^tg* in each array, of which *Ctbp1*, *Jun* and *Wnt7A*, *Bmp2*, *Tgfbi* and *Bmp5* had significant *p*-values. Inhibin alpha was the only gene up-regulated in *Sost^tg* embryos, but no BMP-related transcripts were significantly up-regulated in *Sost^-/-*. In contrast, while no WNT-related transcripts were elevated in *Sost^tg*, *Tcf3* transcription factor, a terminal component of the WNT-signaling pathway that has been shown to function as a repressor (Cole et al., 2008), was significantly up-regulated in *Sost^-/-*. The upregulation of a repressor may explain the mild effect on downstream WNT-targets, suggesting a protective auto-regulatory mechanism for an overactive WNT-pathway in the absence of *Sost* in the limb. *Tcf3* potentially curbs the overactive WNT-signaling due to elevated levels of *Wnt5A* and *Wnt7A* transcripts and activated β-*catenin* protein detected by *in situ* and immunohistochemistry, respectively (data not shown).

To address how SOST interferes with WNT signaling regionally in the limb, we crossed the *SOST* gain-of-function transgene to the WNT reporter *BatGal* mouse (Maretto et al., 2003) and examined WNT responsiveness in the ectoderm, mesenchyme and apical ectodermal ridge of the limb. At embryonic day 10.5 the *LacZ* stain of limb buds viewed in whole *BatGal* and *Sost^tg;BatGal* embryos initially looked indistinguishable and consistent with previously published limb patterns (Maretto et al., 2003), where the dominant expression of *LacZ* is in the AER (Fig. 5A,A′). Upon clearing, dissecting the limb buds and examining *LacZ* expression at higher magnification, and in sections, we observed a decrease in *LacZ* positive cells in both the dorsal and ventral ectoderm and mesenchyme (Fig. 5B-F and B′-F′), within or immediately adjacent to the ectoderm that expresses the highest levels of SOST (Fig. 5G). These results suggest that ectodermal derived SOST inhibits WNT signaling in both the ectoderm and the neighboring mesenchyme. β-catenin is critical for transducing canonical WNT signals to the nucleus of responding cells, where it participates with Lef/Tcf transcription factors in the activation of downstream target genes (Behrens et al. 1996; Molenaar et al. 1996). It has been previously reported that the removal of β-catenin from the limb bud ectoderm results in severe limb defects characterized by lack of hindlimbs and severely truncated forelimbs (Barrow et al., 2003). These findings support the notion that ectodermal WNT signaling is required for proper AER function. While the *BatGal* mice are limiting in this regard, since they express *LacZ* at very low levels in the ectoderm, our results favor the conclusion that WNT signaling in both the ectoderm and the underling mesenchyme is abolished by SOST overexpression.

WNT signaling in the distal mesenchyme is required for anterior-posterior patterning

Our data shows that elevated levels of SOST impair limb patterning along the A-P axis, where the most posterior digit 5 and the most posterior zeugopod element, the ulna, are often absent or abnormal in *Sost^tg*. We attribute these effects to excessive inhibition of WNT signaling,

resulting in misregulation of genes in the two key limb centers, the zone of polarizing activity and the apical ectodermal ridge. Using the WNT signaling reporter *BatGal* we were able to show that ectodermal expressed SOST suppresses WNT signaling both ventrally and dorsally, with the most dramatic downregulation on the ventral side (where SOST is more highly expressed) where *BatGal* transgene signal is completely obliterated in the distal ectoderm and mesenchyme. On the dorsal side, *BatGal* transgene is expressed both in the proximal and distal mesenchyme (and in the ectoderm at very low levels), and consistent with SOST crescent moon expression pattern, *BatGal* transgene is repressed by SOST primarily in the distal region (mesenchyme and ectoderm). *BatGal*, as previously reported, is also expressed in the AER, region devoid of SOST expression, and in our gain of function allele we observe an enhancement in *LacZ* AER expression (Fig. 5B′, D′, F′; black arrow) when SOST is overexpressed in the neighboring ectoderm. Based on these changes in expression pattern of the WNT reporter we can speculate that a net reduction in WNT signaling in the distal mesenchyme and ectoderm (both from the ventral and dorsal regions), results in an overall reduction of SHH expression level in the ZPA, suggesting that WNT signaling in distal mesenchyme/ectoderm is required for either establishing or maintaining SHH expression in the posterior mesenchyme of the developing limb. Since SHH turns on at E9.75, and most of our analysis was carried out at E10.5, we cannot differentiate between these two possibilities, nor can we determine if there is a delay in SHH activation. SHH has also been recently shown to be directly affected by β-catenin signaling, in that reduced β-catenin signaling also directly reduces SHH expression (Miyagawa et al., 2009). Our findings are in support of WNT signaling acting upstream of SHH and positively regulating SHH transcription.

In parallel, we observed gene expression changes in the AER, where both *Fgf8* and *Fgf4* were found to be significantly repressed (Fig. 2E-L) in response to elevated levels of SOST. Since SOST is excluded from the AER, there are several alternate possibilities of how these molecular changes could have emerged. One possibility is that ectodermally expressed SOST inhibits ectodermal WNT signaling, to interrupt the WNT3/β-catenin/FGF regulatory loop shown to be essential for AER establishment and maintenance (Barrow et al., 2003; Hill et al., 2006). The limb bud ectoderm represents a major source of WNT ligands (Witte et al., 2009), therefore it is possible that SOST prevents WNT ligands such as WNT3 from binding to the LRP5/6 receptors within the ectoderm to attenuate WNT signaling in this tissue. Barrow *et al.* has shown that when they conditionally removed either *Wnt3* or β-catenin from the limb ectoderm using Msx2Cre, the mice display severe limb defects highly similar to both $Sost^{tg}$ and $Lrp6^{-/-}$ limbs. In addition, Hill et al. observed that loss of mesenchymal β-catenin activity in the developing limb bud resulted in reduced expression of AER marker genes despite persistent β-catenin activity in the AER of the developing limb. While they reported severe limb truncations, we report varying degrees of posterior limb defects, and no distal truncations. This is likely due to the timing of and the extent of the loss of β-catenin activity, since in our model the loss of β-catenin /WNT signaling in the mesenchyme is incomplete, resulting in a less severe phenotype. While we observed very low levels of ectodermal *LacZ* expression in the *BatGal* mice, we can't rule out that WNT signaling is not affected in the ectoderm, since our results are constrained by the restricted expression pattern of the *BatGal* transgene, which may not fully recapitulate the endogenous WNT activity.

Since limb development proceeds as a tightly coordinated series of morphogenic exchanges between various signaling centers, with very little cell autonomous activity, our results could also be explained as a modification of the ectoderm-ZPA-AER regulatory loop, where ectodermal and/or mesenchymal WNT signaling is required for SHH activity, and a dramatic reduction in SHH (we found SHH to be expressed at ~20% of normal levels in $Sost^{tg}$ and $Lrp6^{-/-}$ limb buds; Fig. 4A) interferes with both ZPA and AER function. The proposed model of SOST action is similar and consistent with previously reported WNT signaling in the limb, whereby epithelial-mesenchymal interactions allow for transduction of signaling effects into

neighboring tissues (ten Berge, et al., 2008). It has also been shown that SHH protein is present not only as a posterior gradient in the mesenchyme but also diffuses to the ectoderm, and that posterior derived skin cells are derived from SHH-responsive cells (Gritli-Linde et al. 2001, Ahn and Joyner, 2004). Our results suggest that SOST is secreted by ectoderm and acts on the adjacent mesenchymal cells, a mode of action consistent with SOST's role during bone metabolism where osteocytes deeply buried in the bone secrete SOST, which travels to the surface of the bone where osteoblasts reside and inhibit their mineralization function (Balemans et al., 2001;Brunkow et al., 2001;Li et al., 2008a;van Bezooijen et al., 2004).

The changes in expression seen in *BatGal* and *Grem1* in the presence of the *SOST* transgene would suggest that there are dorso-ventral patterning defects as well. No obvious dorsal-ventral mispatterning was observed in Sost^{tg} mice. However, Sost^{tg}; Lrp6$^{+/-}$ mice did display ventralization of the dorsal autopod in the form of ectopic nails on the dorsal surface, and Sost$^{-/-}$ mice displayed ectopic pigment and hair on the ventral autopod (data not shown), suggesting dorsalization, which are consistent with perturbations in WNT signaling presented in Fig. 5.

Our findings are also consistent with recent reports that BMP signaling negatively regulates bone mass by induction of sclerostin which then inhibits the canonical WNT pathway (Kamiya et al., 2008). When Sost^{tg} mice were crossed to *Grem1* mice which have limb defects as a direct result of overactive BMP signaling, SOST failed to compensate for the loss of *Grem1* and zeugopod and autopod formation was even further impaired. In contrast, when Sost^{tg} mice were crossed to Lrp5$^{+/-}$ and Lrp6$^{+/-}$ mice, Sost^{tg};Lrp6$^{+/-}$ compound mice displayed defects that are more severe than those in Lrp5$^{-/-}$;Lrp6$^{+/-}$ limbs, while the absence of *Sost* in Sost$^{-/-}$;Lrp6$^{-/-}$ limbs dramatically improves skeletal patterning, providing genetic evidence that *Sost* functions as a WNT antagonist during limb skeletogenesis. While our findings establish SOST as a WNT antagonist in the limb by these genetic criteria, we cannot rule out the possibility that SOST has some BMP-antagonistic activity, as previously suggested. One possible reason for the discrepancies between the previous data, where SOST was shown to inhibit the BMP pathway could be explained by a dual, context-dependent role of SOST, such that SOST affinity for one pathway is tissue dependent.

Since WNT signaling is implicated in a multitude of processes and WNT ligands are broadly expressed spatially and temporarily during vertebrate limb development, inhibitors of WNT signaling play an important role as gatekeepers of signal transduction and cell-cell communication across tissues. It is increasingly clear that a balanced combination of ligand expression and antagonistic regulation is required to ensure accurate WNT signaling and therefore proper limb outgrowth, patterning and cartilage differentiation. Here we have shown that in addition to the pervasive high bone mass phenotype recorded for sclerosteosis patients and *Sost* knock-out mice, SOST also contributes to the robustness of limb patterning signals by weakening the signal transduced through the LRP/6 receptors.

Materials and Methods

Generation of compound mice

Sost^{tg}, *Grem1*, *Lrp5*, *Lrp6*, *BatGal* and *Sost* mutant mice have been previously described (Holmen et al., 2004; Khokha et al., 2003; Li et al., 2008a; Loots et al., 2005; Maretto et al., 2003). *Sost* KOMP knockout mice were generated by a *LacZ* replacement of the entire *Sost* open reading frame. Sost^{tg} or Sost$^{-/-}$ mice were mated to *BatGal* individual knockout strains and the progeny were genotyped by PCR (primer sequences and PCR conditions available upon request). Progeny were selected for Sost^{tg}; *BatGal*, Sost^{tg};hets or double hets and were mated to each other in timed matings; embryos were collected at E9.5, E10.5, E11.5, E12.5, E14.5, and/or E17.5, depending on the desired analysis, and the embryonic sac was genotyped

by PCR. E0.5 of gestation was considered as noon on the day a visual copulatory plug was observed. Staging of embryos was verified where possible (prior to E12.5) by counting somites. All animal experiments were carried out in accordance with guidelines set by the Animal Care and Use Committee at University of California-Berkeley and Lawrence Livermore National Laboratory.

Whole mount *in situ* hybridization—were carried out using standard procedures (Khokha et al., 2003). Species specific sequences of human and mouse *Sost* were cloned from the 3′ UTR region of each cDNA (human Sost NM_02537.2; mouse Sost NM_024449.4). Briefly, digoxigenin-labeled antisense RNA probes were generated to the desired RNA sequence, and hybridized to wholemount embryos. Expression was visualized by biding BM Purple (Roche). Antisense RNA probes for *Grem1* (MluI-SacII fragment of NM_011824), *Fgf8* [PstI 3′ cDNA and UTR fragment of NM_010205; see (Crossley and Martin, 1995)], *Fgf4* (NM_01202.5) and *Shh* [MscI-NarI fragment of NM_009170; see (Echelard et al., 1993)] were generated as described (Hogan et al., 1994) with the following modification: proteinase K digestion was omitted for ectodermal or AER probes. A minimum of 4 embryos were used per genotype, per experiment. Wild type controls were obtained from the same litter, whenever possible.

***LacZ* stains**—Embryos were dissected free of extraembryonic membranes into ice-cold 1× phosphate-buffered saline (PBS), pH 7.3. Embryos were fixed in 2% paraformaldehyde, 0.2% glutaraldehyde in 1× PBS, 2mM MgCl2 at 4°C for 30 minutes to 1 hour, followed by extensive rinsing in 1× PBS, 2mM MgCl2. Embryos were stained for 4 hours (*BatGal*) at RT or overnight (*Sost$^{-/-}$*) at 4°C in X-gal stain: 1mg/ml X-gal; 2mM MgCl2; 5mM EGTA; 0.02% Nonidet P-40; 5mM potassium ferrocyanide; 5mM potassium ferricyanide; in 1× PBS, pH 7.3. After staining, embryos were post-fixed in 4% paraformaldehyde in 1× PBS, pH 7.3 at 4°C, and then cleared in glycerol for photography.

Skeletal Preparations—were made of E17.5 day mouse embryos using Alcian Blue 8GX for cartilage and Alizarin Red S for bone following established protocols. Embryos were dissected free of internal organs, and skin, and fixed in 95% ethanol followed by stain in 0.05% Alcian Blue 8GX, 80% ethanol, 20% glacial acetic acid. Excess stain was washed out and embryos were then stained in 60 mg/L Alizarin Red S, 1% potassium hydroxide (KOH), 25% glycerol followed by clearing in 1% KOH, 25% glycerol and storage in glycerol for photography. For skeletal preparation, whole litters were analyzed.

Quantitative rtPCR

Total RNA was isolated from limb-buds using Qiagen methods and reverse-transcribed into cDNA (Superscript II, Gibco). Quantitative rtPCR expression analysis was performed using an ABI Prism 7900HT sequence detection system, TaqMan® Universal PCR Master mix, eukaryotic *18S* rRNA pre-developed TaqMan® assay reagent for normalization and TaqMan® Assay-on-Demand™ products for mouse and human *Sost*, and murine *Fgf4*, *Fgf8*, *Shh*, *Grem1*, *dHand*, *Axin2* (Applied Biosystems). For microarrays, 250 to 1000 ng of total RNA from E10.5 forelimbs was converted into cDNA using RT2 First Strand Kit (SA Biosciences), which included a genomic DNA elimination step.

Supplementary Material

Refer to Web version on PubMed Central for supplementary material.

Acknowledgments

References

Ahn S, Joyner AL. Dynamic changes in the response of cells to positive hedgehog signaling during mouse limb patterning. Cell 2004;118:505–16. [PubMed: 15315762]

Balemans W, Ebeling M, Patel N, Van Hul E, Olson P, Dioszegi M, Lacza C, Wuyts W, Van Den Ende J, Willems P, Paes-Alves AF, Hill S, Bueno M, Ramos FJ, Tacconi P, Dikkers FG, Stratakis C, Lindpaintner K, Vickery B, Foernzler D, Van Hul W. Increased bone density in sclerosteosis is due to the deficiency of a novel secreted protein (SOST). Hum Mol Genet 2001;10:537–43. [PubMed: 11181578]

Bandyopadhyay A, Tsuji K, Cox K, Harfe BD, Rosen V, Tabin CJ. Genetic analysis of the roles of BMP2, BMP4, and BMP7 in limb patterning and skeletogenesis. PLoS Genet 2006;2:e216. [PubMed: 17194222]

Barrow JR, Thomas KR, Boussadia-Zahui O, Moore R, Kemler R, Capecchi MR, McMahon AP. Ectodermal Wnt3/beta-catenin signaling is required for the establishment and maintenance of the apical ectodermal ridge. Genes Dev 2003;17:394–409. [PubMed: 12569130]

Benazet JD, Bischofberger M, Tiecke E, Goncalves A, Martin JF, Zuniga A, Naef F, Zeller R. A self-regulatory system of interlinked signaling feedback loops controls mouse limb patterning. Science 2009;323:1050–3. [PubMed: 19229034]

Ten Berge D, Brugmann SA, Helms JA, Nusse R. Wnt and FGF signals interact to coordinate growth with cell fate specification during limb development. Development 2008;135:3247–3257. [PubMed: 18776145]

Brunet LJ, McMahon JA, McMahon AP, Harland RM. Noggin, cartilage morphogenesis, and joint formation in the mammalian skeleton. Science 1998;280:1455–7. [PubMed: 9603738]

Brunkow ME, Gardner JC, Van Ness J, Paeper BW, Kovacevich BR, Proll S, Skonier JE, Zhao L, Sabo PJ, Fu Y, Alisch RS, Gillett L, Colbert T, Tacconi P, Galas D, Hamersma H, Beighton P, Mulligan J. Bone dysplasia sclerosteosis results from loss of the SOST gene product, a novel cystine knot-containing protein. Am J Hum Genet 2001;68:577–89. [PubMed: 11179006]

Cole MF, Johnstone SE, Newman JJ, Kagey MH, Young RA. Tcf3 is an integral component of the core regulatory circuitry of embryonic stem cells. Genes Dev 2008;22:746–55. [PubMed: 18347094]

Cremin BJ. Sclerosteosis in children. Pediatr Radiol 1979;8:173–7. [PubMed: 471562]

Crossley PH, Martin GR. The mouse Fgf8 gene encodes a family of polypeptides and is expressed in regions that direct outgrowth and patterning in the developing embryo. Development 1995;121:439–51. [PubMed: 7768185]

Duprez DM, Coltey M, Amthor H, Brickell PM, Tickle C. Bone morphogenetic protein-2 (BMP-2) inhibits muscle development and promotes cartilage formation in chick limb bud cultures. Dev Biol 1996;174:448–52. [PubMed: 8631514]

Echelard Y, Epstein DJ, St-Jacques B, Shen L, Mohler J, McMahon JA, McMahon AP. Sonic hedgehog, a member of a family of putative signaling molecules, is implicated in the regulation of CNS polarity. Cell 1993;75:1417–30. [PubMed: 7916661]

Ellies DL, Viviano B, McCarthy J, Rey JP, Itasaki N, Saunders S, Krumlauf R. Bone density ligand, Sclerostin, directly interacts with LRP5 but not LRP5G171V to modulate Wnt activity. J Bone Miner Res 2006;21:1738–49. [PubMed: 17002572]

Galceran J, Farinas I, Depew MJ, Clevers H, Grosschedl R. Wnt3a-/--like phenotype and limb deficiency in Lef1(-/-)Tcf1(-/-) mice. Genes Dev 1999;13:709–17. [PubMed: 10090727]

Hill TP, Taketo MM, Birchmeier W, Hartmann C. Multiple roles of mesenchymal β-catenin during murine limb patterning. Development 2006;133:1219–1229. [PubMed: 16495310]

Hogan, BL.; Beddington, R.; Costantini, F.; Lacey, E. Manipulating the Mouse Embryo: A Laboratory Manual. 2nd. Cold Spring Harbor Press; New York: 1994.

Holmen SL, Giambernardi TA, Zylstra CR, Buckner-Berghuis BD, Resau JH, Hess JF, Glatt V, Bouxsein ML, Ai M, Warman ML, Williams BO. Decreased BMD and limb deformities in mice carrying mutations in both Lrp5 and Lrp6. J Bone Miner Res 2004;19:2033–40. [PubMed: 15537447]

Itasaki N, Jones CM, Mercurio S, Rowe A, Domingos PM, Smith JC, Krumlauf R. Wise, a context-dependent activator and inhibitor of Wnt signalling. Development 2003;130:4295–305. [PubMed: 12900447]

Jho EH, Zhang T, Domon C, Joo CK, Freund JN, Costantini F. Wnt/beta-catenin/Tcf signaling induces the transcription of Axin2, a negative regulator of the signaling pathway. Mol Cell Biol 2002;22:1172–83. [PubMed: 11809808]

Joyner A, Wall N. Immunohistochemistry of Whole-Mount Mouse Embryos. Cold Spring Harbor Protocols 2008;3:4820.

Kamiya N, Ye L, Kobayashi T, Mochida Y, Yamauchi M, Kronenberg HM, Feng JQ, Mishina Y. BMP signaling negatively regulates bone mass through sclerostin by inhibiting the canonical Wnt pathway. Development 2008;135:3801–11. [PubMed: 18927151]

Kassai Y, Munne P, Hotta Y, Penttila E, Kavanagh K, Ohbayashi N, Takada S, Thesleff I, Jernvall J, Itoh N. Regulation of mammalian tooth cusp patterning by ectodin. Science 2005;309:2067–70. [PubMed: 16179481]

Khokha MK, Hsu D, Brunet LJ, Dionne MS, Harland RM. Gremlin is the BMP antagonist required for maintenance of Shh and Fgf signals during limb patterning. Nat Genet 2003;34:303–7. [PubMed: 12808456]

Kraus P, Fraidenraich D, Loomis CA. Some distal limb structures develop in mice lacking Sonic hedgehog signaling. Mech Dev 2001;100:45–58. [PubMed: 11118883]

Laurikkala J, Kassai Y, Pakkasjarvi L, Thesleff I, Itoh N. Identification of a secreted BMP antagonist, ectodin, integrating BMP, FGF, and SHH signals from the tooth enamel knot. Dev Biol 2003;264:91–105. [PubMed: 14623234]

Li X, Ominsky MS, Niu QT, Sun N, Daugherty B, D′Agostin D, Kurahara C, Gao Y, Cao J, Gong J, Asuncion F, Barrero M, Warmington K, Dwyer D, Stolina M, Morony S, Sarosi I, Kostenuik PJ, Lacey DL, Simonet WS, Ke HZ, Paszty C. Targeted Deletion of the Sclerostin Gene in Mice Results in Increased Bone Formation and Bone Strength*. J Bone Miner Res. 2008a

Li X, Ominsky MS, Warmington KS, Morony S, Gong J, Cao J, Gao Y, Shalhoub V, Tipton B, Haldankar R, Chen Q, Winters A, Boone T, Geng Z, Niu QT, Ke HZ, Kostenuik PJ, Simonet WS, Lacey DL, Paszty C. Sclerostin Antibody Treatment Increases Bone Formation, Bone Mass and Bone Strength in a Rat Model of Postmenopausal Osteoporosis *. J Bone Miner Res. 2008b

Li X, Zhang Y, Kang H, Liu W, Liu P, Zhang J, Harris SE, Wu D. Sclerostin binds to LRP5/6 and antagonizes canonical Wnt signaling. J Biol Chem 2005;280:19883–7. [PubMed: 15778503]

Lin C, Jiang X, Dai Z, Guo X, Weng T, Wang J, Li Y, Feng G, He L. Sclerostin mediates bone response to mechanical unloading through antagonizing Wnt/β-catenin signaling. J Bone Miner Res 2009;24:1651–1661. [PubMed: 19419300]

Litingtung Y, Dahn RD, Li Y, Fallon JF, Chiang C. Shh and Gli3 are dispensable for limb skeleton formation but regulate digit number and identity. Nature 2002;418:979–83. [PubMed: 12198547]

Loots GG, Kneissel M, Keller H, Baptist M, Chang J, Collette NM, Ovcharenko D, Plajzer-Frick I, Rubin EM. Genomic deletion of a long-range bone enhancer misregulates sclerostin in Van Buchem disease. Genome Res 2005;15:928–35. [PubMed: 15965026]

Macias D, Ganan Y, Sampath TK, Piedra ME, Ros MA, Hurle JM. Role of BMP-2 and OP-1 (BMP-7) in programmed cell death and skeletogenesis during chick limb development. Development 1997;124:1109–17. [PubMed: 9102298]

Maretto S, Cordenonsi M, Dupont S, Braghetta P, Broccoli V, Hassan AB, Volpin D, Bressan GM, Piccolo S. Mapping Wnt/beta-catenin signaling during mouse development and in colorectal tumors. Proc Natl Acad Sci U S A 2003;100:3299–304. [PubMed: 12626757]

Michos O, Panman L, Vintersten K, Beier K, Zeller R, Zuniga A. Gremlin-mediated BMP antagonism induces the epithelial-mesenchymal feedback signaling controlling metanephric kidney and limb organogenesis. Development 2004;131:3401–10. [PubMed: 15201225]

Miyagawa S, Moon A, Haraguchi R, Inoue C, Harada M, Nakahara C, Suzuki K, Matsumaru D, Kaneko T, Matsuo I, Yang L, Taketo MM, Iguchi T, Evans SM, Yamada G. Dosage-dependent hedgehog signals integrated with Wnt/b-catenin signaling regulate external genitalia formation as an appendicular program. Development 2009;136:3969–3978. [PubMed: 19906864]

Niehrs C. Function and biological roles of the Dickkopf family of Wnt modulators. Oncogene 2006;25:7469–81. [PubMed: 17143291]

Niemann S, Zhao C, Pascu F, Stahl U, Aulepp U, Niswander L, Weber JL, Muller U. Homozygous WNT3 mutation causes tetra-amelia in a large consanguineous family. Am J Hum Genet 2004;74:558–63. [PubMed: 14872406]

Panman L, Galli A, Lagarde N, Michos O, Soete G, Zuniga A, Zeller R. Differential regulation of gene expression in the digit forming area of the mouse limb bud by SHH and gremlin 1/FGF-mediated epithelial-mesenchymal signalling. Development 2006;133:3419–28. [PubMed: 16908629]

Parr BA, McMahon AP. Dorsalizing signal Wnt-7a required for normal polarity of D-V and A-P axes of mouse limb. Nature 1995;374:350–3. [PubMed: 7885472]

Pinson KI, Brennan J, Monkley S, Avery BJ, Skarnes WC. An LDL-receptor-related protein mediates Wnt signalling in mice. Nature 2000;407:535–8. [PubMed: 11029008]

Pinzone JJ, Hall BM, Thudi NK, Vonau M, Qiang YW, Rosol TJ, Shaughnessy JD Jr. The role of Dickkopf-1 in bone development, homeostasis, and disease. Blood 2009;113:517–25. [PubMed: 18687985]

Scherz PJ, Harfe BD, McMahon AP, Tabin CJ. The limb bud Shh-Fgf feedback loop is terminated by expansion of former ZPA cells. Science 2004;305:396–9. [PubMed: 15256670]

Sutherland MK, Geoghegan JC, Yu C, Turcott E, Skonier JE, Winkler DG, Latham JA. Sclerostin promotes the apoptosis of human osteoblastic cells: a novel regulation of bone formation. Bone 2004;35:828–35. [PubMed: 15454089]

van Bezooijen RL, Roelen BA, Visser A, van der Wee-Pals L, de Wilt E, Karperien M, Hamersma H, Papapoulos SE, ten Dijke P, Lowik CW. Sclerostin is an osteocyte-expressed negative regulator of bone formation, but not a classical BMP antagonist. J Exp Med 2004;199:805–14. [PubMed: 15024046]

van Bezooijen RL, Svensson JP, Eefting D, Visser A, van der Horst G, Karperien M, Quax PH, Vrieling H, Papapoulos SE, ten Dijke P, Lowik CW. Wnt but not BMP signaling is involved in the inhibitory action of sclerostin on BMP-stimulated bone formation. J Bone Miner Res 2007;22:19–28. [PubMed: 17032150]

Winkler DG, Sutherland MK, Geoghegan JC, Yu C, Hayes T, Skonier JE, Shpektor D, Jonas M, Kovacevich BR, Staehling-Hampton K, Appleby M, Brunkow ME, Latham JA. Osteocyte control of bone formation via sclerostin, a novel BMP antagonist. Embo J 2003;22:6267–76. [PubMed: 14633986]

Witte F, Dokas J, Neuendorf F, Mundlos S, Stricker S. Comprehensive expression analysis of all Wnt genes and their major secreted antagonists during mouse limb development and cartilage differentiation. Gene Expr Patterns 2009;9:215–23. [PubMed: 19185060]

Woods CG, Stricker S, Seemann P, Stern R, Cox J, Sherridan E, Roberts E, Springell K, Scott S, Karbani G, Sharif SM, Toomes C, Bond J, Kumar D, Al-Gazali L, Mundlos S. Mutations in WNT7A cause a range of limb malformations, including Fuhrmann syndrome and Al-Awadi/Raas-Rothschild/Schinzel phocomelia syndrome. Am J Hum Genet 2006;79:402–8. [PubMed: 16826533]

Yanagita M. BMP antagonists: their roles in development and involvement in pathophysiology. Cytokine Growth Factor Rev 2005;16:309–17. [PubMed: 15951218]

Zuniga A, Haramis AP, McMahon AP, Zeller R. Signal relay by BMP antagonism controls the SHH/FGF4 feedback loop in vertebrate limb buds. Nature 1999;401:598–602. [PubMed: 10524628]
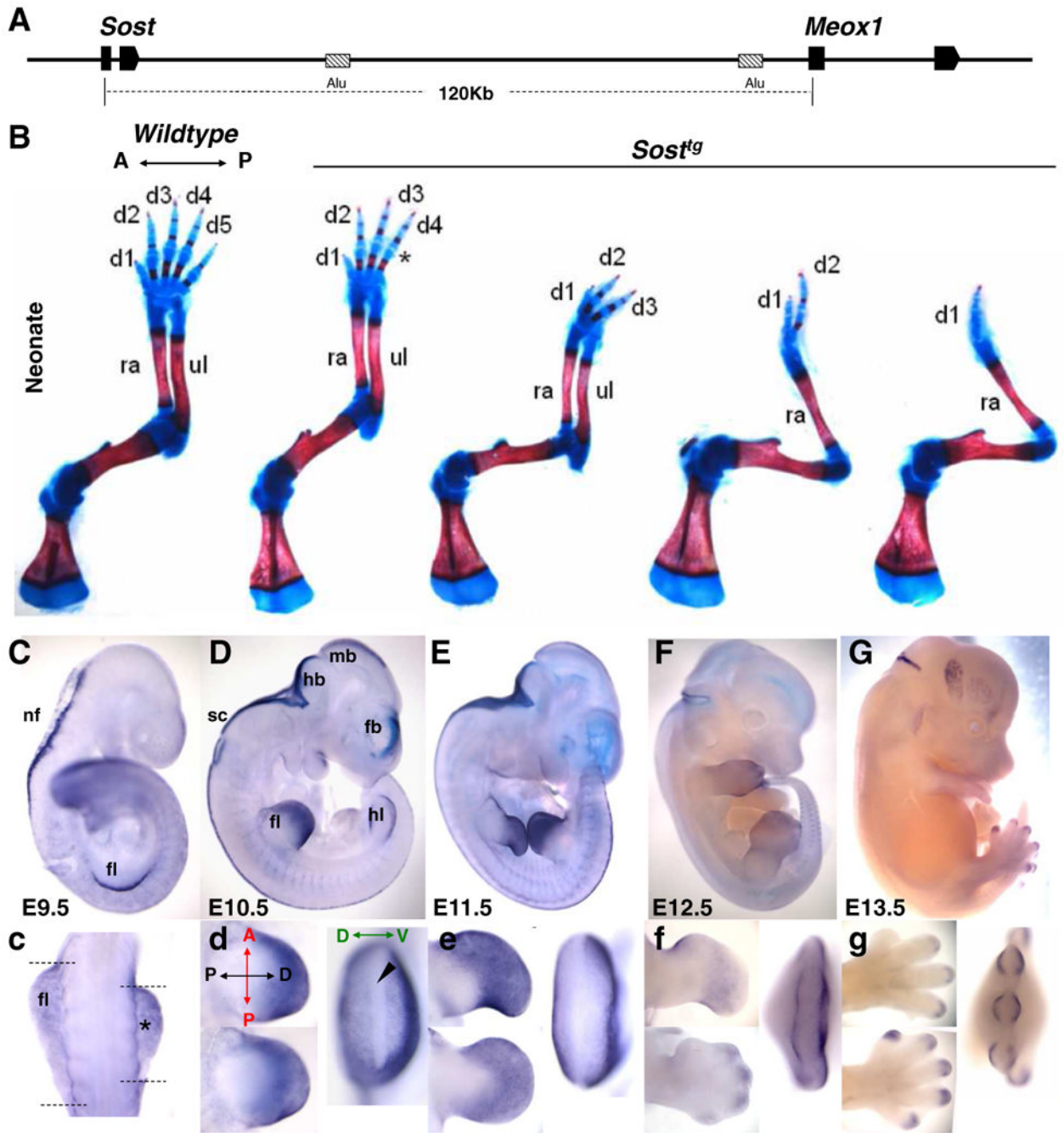
Figure 1. Limb defects and human *Sost* expression in the *Sost^tg* developing limb
(**A**) A 158kb human transgene spanning the *Sost* and *Meox1* transcript was used to generate the *Sost^tg* gain-of-function allele (Loots et al., 2005). (**B**) Skeletal preparations of E17.5 wild type and *Sost^tg* embryos where *Sost* gain-of-function results in progressive loss of skeletal elements from posterior to anterior. A limb was scored as abnormal if it fell outside of the range observed in wild type samples; 117 total animals were scored consisting of 77 *Sost^tg* and 40 wild type. (*d* digit, *ra* radius, *ul* ulna, *tg* transgenic, *wt* wild type). (**C-F**) Human *Sost* expression was visualized by *in situ* hybridization using a human specific *Sost* probe, in a time-course panel of E9.5 to E12.5 *Sost^tg* embryos. At each time point whole embryo (C-F), and dorsal limb and AER views are provided (c-f). Dorsal limb bud views are provided for two different

Sost^{tg} littermate embryos at each time point, where the top limb corresponds to a severely affected embryos and the bottom limb is from a *Sost^{tg}* embryo that is morphologically indistinguishable from a wild type limb bud). Asterisk highlights developmentally delayed mutant limb bud; arrowhead points to AER. *fl* forelimb, *hl* hindlimb, *nf* neural folds, *sc* spinal cord, *mb* midbrain, *fb* forebrain, *def* defective, *tg* transgenic
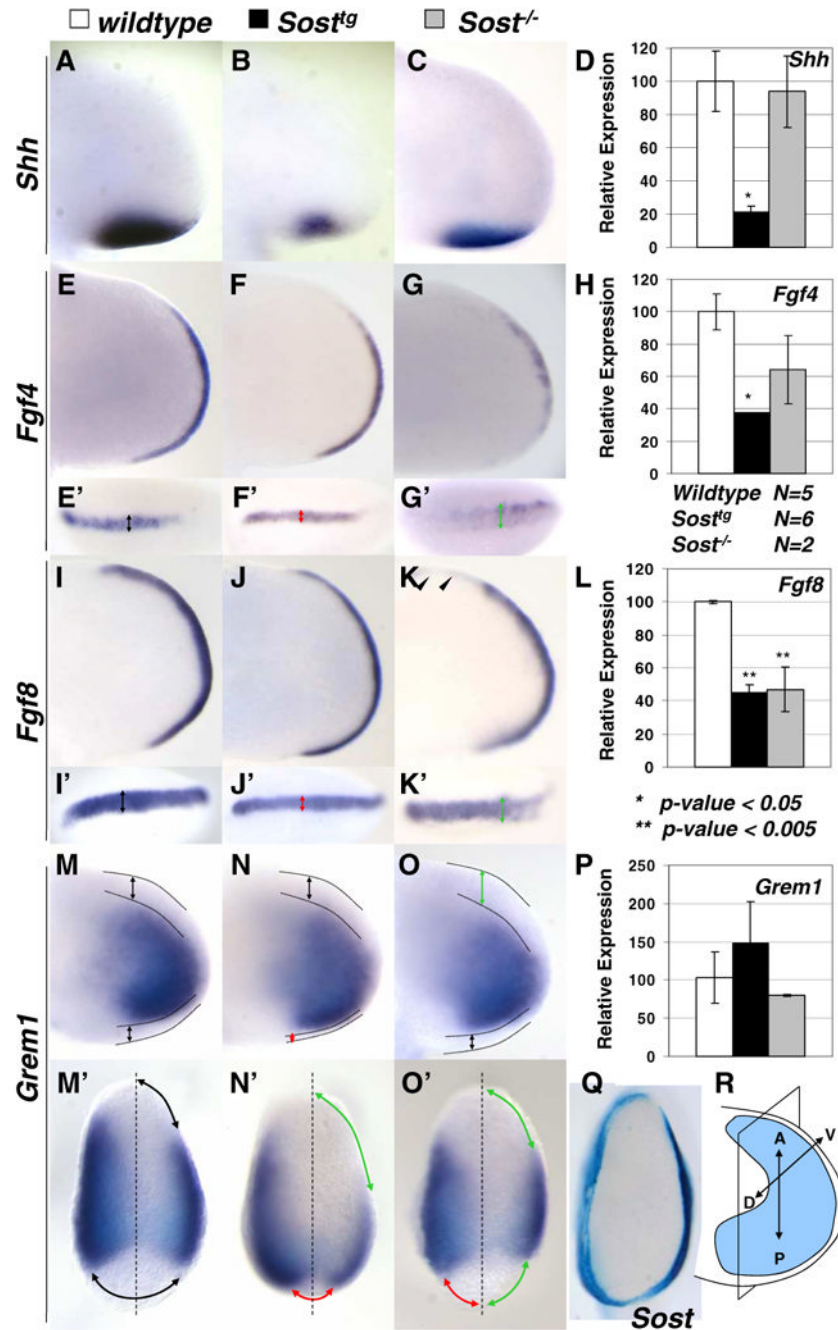
Figure 2. Repression of ZPA and AER genes in *Sost^tg*
(**A-D**) *Shh*, (**E-H**) *Fgf4* and (**I-L**) *Fgf8* were significantly down-regulated in *Sost^tg* E10.5 limb buds. *Shh* was down to 20% its normal expression level in *Sost^tg*, but unaffected in *Sost^-/-* embryos (D). *Fgf4* and *Fgf8* were down-regulated in both *Sost^tg* and *Sost^-/-* embryos (H, L); the AER width was dependent on *Sost* levels, such that high levels of *Sost* limited its domain (J′, red arrow), while the absence of *Sost* disorganized and expanded it dorso-ventrally (K′, green arrow). (**M-P**) *Grem1*, a mesenchymal marker, while quantitatively appeared unaffected (P), its expression domain (N, O) was altered in both Gain- and Loss-of-Function embryos. In *Sost^tg* embryos *Grem1* domain was expanded posteriorly (N′, red arrow), along with an anterior reduction on the ventral side (N′, green arrow). In *Sost^-/-* embryos similar asymmetric, but more

subtle changes were observed (O′). **(Q)** Sost expression is restricted to the limb bud ectoderm. **(R)** Limb bud sections were carried out as illustrated.
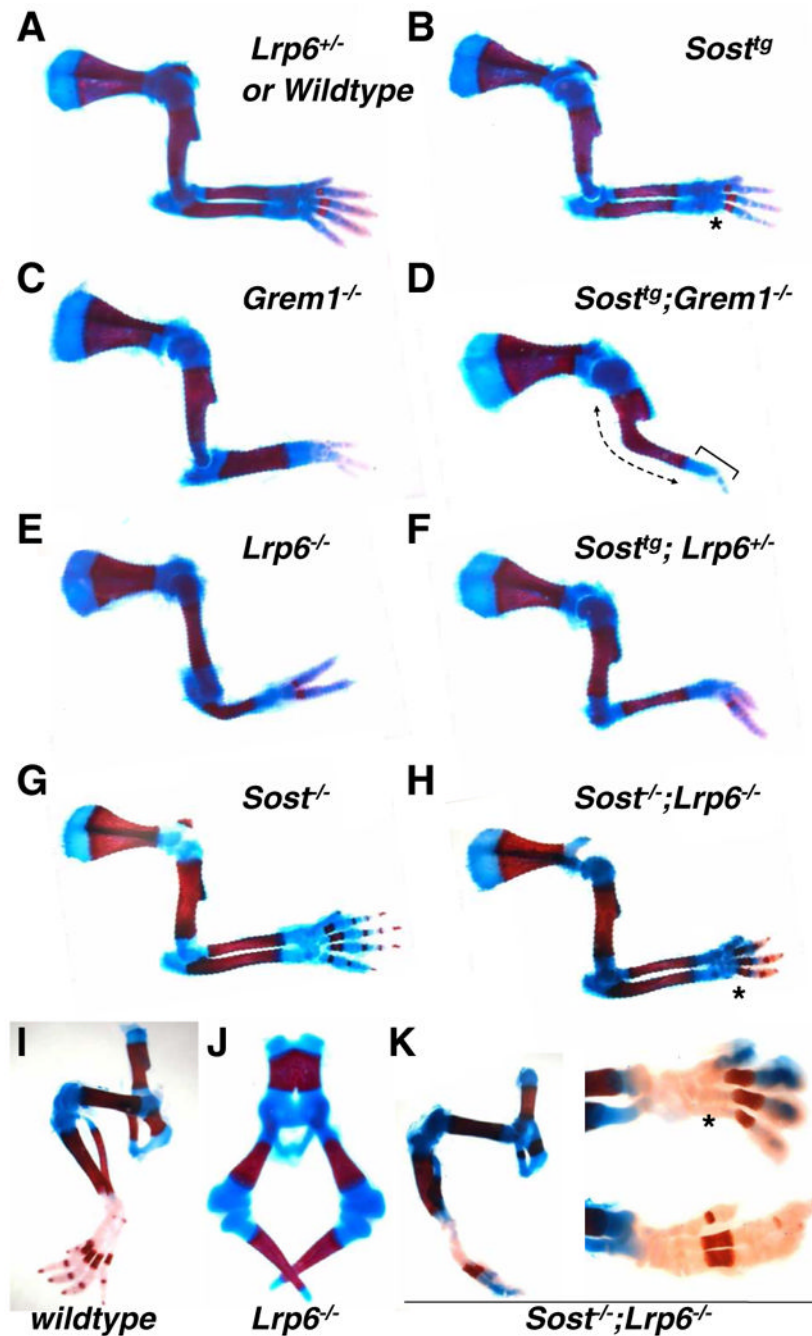
Figure 3. *Sost* **gain-of-function modifies both** *Grem1*$^{-/-}$ **and** *Lrp6*$^{-/-}$ **limb phenotypes, but** *Sost* **loss-of-function rescues only** *Lrp6*$^{-/-}$

(A-H) Skeletal preparations of wild type or *Lrp6*$^{+/-}$ (A), *Sost*^{tg} (B), *Grem1*$^{-/-}$ (C), *Sost*^{tg};*Grem1*$^{-/-}$ (D), *Lrp6*$^{-/-}$ (E), *Sost*^{tg};*Lrp6*$^{-/-}$ (F), *Sost*$^{-/-}$ (G) and *Sost*$^{-/-}$;*Lrp6*$^{-/-}$ (H) forelimbs. 40% of *Sost*^{tg};*Grem1*$^{-/-}$ (D) forelimbs lacked an elbow, where the humerus, radius and ulna have formed one skeletal element (arrow) and the wrist and autopod were highly reduced and lack most digits (bracket). While *Lrp6* heterozygous forelimbs were indistinguishable from wild type, *Sost*^{tg} modified the *Lrp6* phenotype (E) such that *Sost*^{tg};*Lrp6*$^{+/-}$ forelimbs were indistinguishable from *Lrp6*$^{-/-}$ (F). Removal of *Sost* in the absence of *Lrp6* receptor resulted in dramatic rescue of *Lrp6*$^{-/-}$ limb phenotype (H).
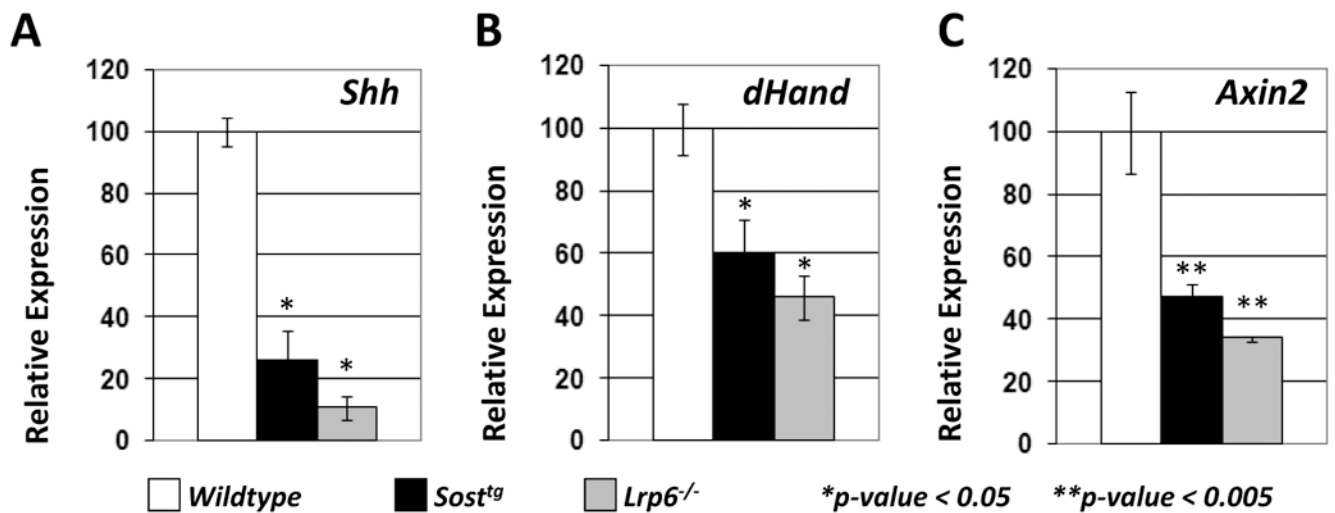
Figure 4. Inhibition of *Shh* and WNT signaling in both *Sost^tg* and *Lrp6^-/-* limb buds
(A-C) Limb bud RNA was isolated from wild type, *Sost^tg* and *Lrp6^-/-* E10.5 limb buds. Normal expression of *Shh* (A) and its downstream transcriptional target *dHand* (B) was dramatically reduced in both *Sost^tg* and *Lrp6^-/-* embryos. Similarly, *Axin2* expression, a downstream target of canonical WNT signaling, was less than 50% of normal levels in both *Sost^tg* and *Lrp6^-/-* embryos (C).
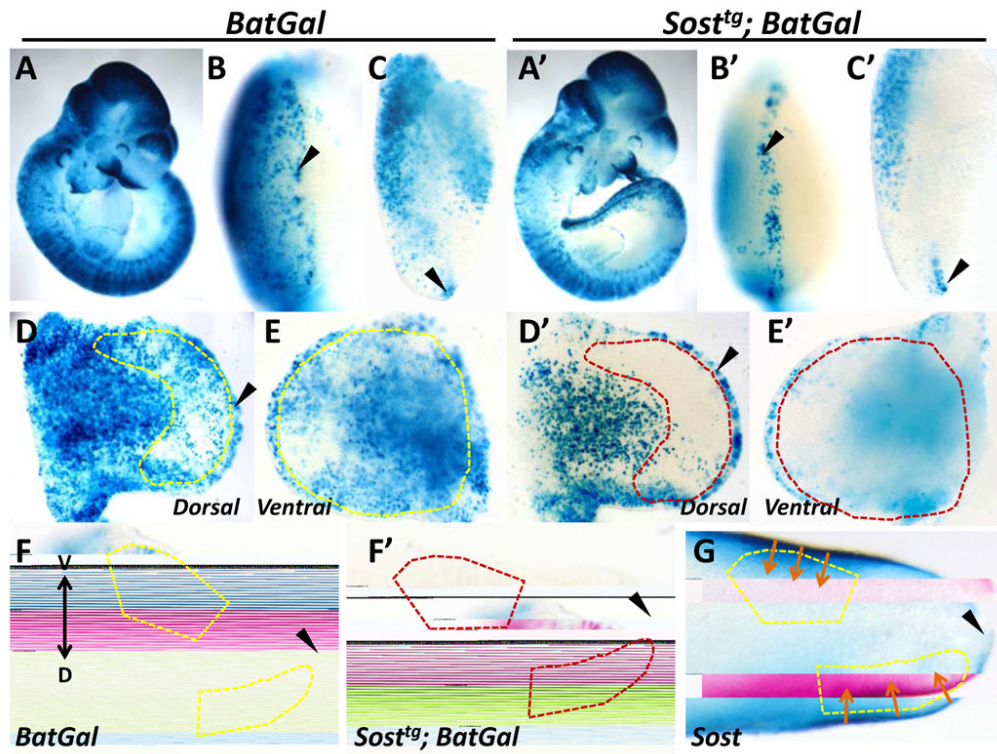
Figure 5. Ectodermal SOST inhibits WNT signaling in the mesenchyme
(A-F) WNT activity in the limb was examined in *BatGal* WNT reporter mice. *LacZ* expression from the *BatGal* WNT reporter transgene was examined in E10.5 wild type (A-F) and *Sost^tg* (A′-F′) embryos in whole mount (A, A′), AER limb views (B, B′), transverse limb sections (C, C′, F, F′), dorsal (D, D′) and ventral (E, E′) limb bud views. Ectodermal derived SOST (G) repressed *BatGal LacZ* reporter expression in the dorsal (D, D′) and ventral ectoderm (E, E′) in a pattern consistent with human *SOST* transgene expression (yellow dashed region). On the ventral side all reporter activity was lost (E′, F′; red dashed region). AER *LacZ* expression was unaffected or enhanced in the presence of *SOST* (B′, D′, F′). Black arrows indicate the AER, the region where *SOST* is absent (G), orange arrows indicate morphogenic activity of ectodermal derived SOST to suppress WNT signaling in the underlining mesenchyme.

Table 1

Genetic analysis of Sost gain-of-function mutations in combination with mutations in members of the Wnt and Bmp signaling pathways

Genotype	N	Forelimb	Hindlimb	Other
			$Sost^{tg} \times Grem1^{-/-}$	
$Sost^{tg}$	6	Normal	Normal	
	13	Loss of digits (3-4d rF, 3-5d lF)	Normal	
	1	Loss of digits (3d bF)	Loss of digits (1d lH)/Loss of fibula (lH)	
$Grem1^{+/-}$	17	Normal	Normal	
$Grem1^{-/-}$	10	Fused radius/ulna	Loss of fibula	
		Loss of digits (3d bF)	Loss of digits (0-3d bH)	
$Sost^{tg};Grem1^{+/-}$	17	Normal	Normal	
	3	Loss of digits (2-4d rF, 3-5d rF)		
	6	Loss of digits (3-4d rF, 3-5d lF)	Loss of digits (3-4d lH)	
$Sost^{tg};Grem1^{-/-}$	6	Fused radius/ulna	Loss of fibula/digits (0-3d bH)	
		Loss of digits (3d bF)		
	4	Fused ulna/shortened humerus	Truncated tibia/ No digits/Loss of fibula	
			$Sost^{tg} \times Lrp5^{-/-}$	
$Sost^{tg}$	14	Normal	Normal	
	16	Loss of digits (2-4d bF)	Normal	
	2	Loss of ulna/digits (2-3d bF)	Loss of digits (1d lH)/Loss of fibula	
$Lrp5^{+/-}$ and $Lrp5^{-/-}$	31	Normal	Normal	
$Sost^{tg};Lrp5^{+/-}$	21	Loss of digits (2-4d rF, 3-4d lF)	Normal	
	3	Loss of ulna/digits (2-4d bF)	Normal	Curly tail
$Sost^{tg};Lrp5^{-/-}$	3	Loss of digits (4d rF)	Normal	
	5	Loss of digits (2-3d bf)	Loss of digits (3-5d bH)	Curly tail; runty; neonate death
			$Sost^{tg} \times Lrp6^{+/-}$	
$Sost^{tg}$	6	Normal	Normal	
	14	Loss of digits (2-4d bF)	Normal	
$Lrp6^{+/-}$	23	Normal	Normal	
$Lrp6^{-/-}$	11	Loss of ulna (lF)/short radius	Truncated femur/No digits	Spina bifida; no tail
		Loss of digits (4d rF, 2d lF)		Abnormal/fused pelvis Cleft jaw/ palate Microcephaly[*]; microopthalmia[*]
$Sost^{tg};Lrp6^{+/-}$	25	Loss of Digits-Mild (2-5d bF, s lF)	Loss of Digits (3-5d bH)	
		Dorsal Ectopic Nails	Dorsal Ectopic Nails	
	9	Loss of Digits-Severe (1-3d bF)	Truncated/No digits	Spina Bifida Curly/truncated tail
			$Lrp5^{-/-} \times Lrp6^{+/-}$	
$Lrp5^{+/-}$ and $Lrp6^{+/-}$	30	Normal	Normal	
$Lrp5^{+/-};Lrp6^{+/-}$	19	Loss of Digits (4d rF, small d5 lF)	Normal	
$Lrp5^{-/-};Lrp6^{+/-}$	7	Loss of Digits (2-3d bF)	Normal	

Genotype	N	Forelimb	Hindlimb	Other
			$Sost^{-/-} \times Lrp6^{+/-}$	
$Sost^{+/-}$ and $Sost^{-/-}$	27	Normal	Normal	
$Lrp6^{+/-}$	22	Normal	Normal	
$Lrp6^{-/-}$	11	Loss of ulna (lF)/short radius	Truncated femur/no fibula	Spina Bifida, no tail
		Loss of digits (4d rF, 2d lF)	Lack of feet	Abnormal/fused pelvis Bilateral cleft jaw/palate Microcephaly[*]; microopthalmia[*]
$Sost^{+/-};Lrp6^{+/-}$	18	Normal	Normal	
$Sost^{-/-};Lrp6^{+/-}$	10	Normal	Normal	
$Sost^{-/-};Lrp6^{-/-}$	8	Loss of digit (4d bF)	Loss of digits (3-4d bH)	Spina bifida, no tail
			Loss of fibula (rH)	Unilateral cleft palate

d digit, F forelimb, H hindlimb, r right, l left, b both, s syndactyly

[*] rescue of phenotype was not quantified in $Sost^{-/-};Lrp6^{-/-}$